*J. Fluid Mech.* (2000), *vol.* 402, *pp.* 225–253. Printed in the United Kingdom



# Turbulent heat and momentum transport on a rotating disk

By CHRISTOPHER J. ELKINS AND JOHN K. EATON
Department of Mechanical Engineering, Stanford University, Stanford, CA 94305, USA

(Received 6 October 1998 and in revised form 4 June 1999)

Measurements in the turbulent momentum and thermal boundary layers on a rotating disk with a uniform heat flux surface are described for Reynolds numbers up to $10^6$. Measurements include mean velocities and temperatures, all six Reynolds stresses, turbulent temperature fluctuations, and three turbulent heat fluxes. The mean velocity profiles have no wake region, but the mean temperature profiles do. The turbulent temperature fluctuations have a large peak in the outer layer, and there is a third turbulent heat flux in the cross-flow direction. Correlation coefficients and structure parameters are not constant across the boundary layer as they are in two-dimensional boundary layers (2DBLs), and their values are lower. The turbulent Prandtl number agrees with 2DBL values in the lower part of the outer region but is reduced from the 2DBL values higher in the boundary layer. In the outer region of the boundary layer, the transport processes differ significantly from what is observed in two-dimensional turbulent boundary layers: ejections dominate the transport of momentum while both ejections and sweeps contribute to the transport of the passive scalar.

## 1. Introduction

The flow on a disk in an otherwise quiescent environment is of interest as a simple flow for investigating three-dimensional turbulent boundary layer (3DTBL) physics and as a benchmark flow that can be used in modelling more complex flows directly relevant to rotating machinery. The flow exhibits skewing of the velocity vector (figure 1) across the boundary layer which is the defining characteristic of 3DTBLs. The skewing develops because a radial pressure gradient cannot be maintained in the infinite quiescent medium leaving nothing to oppose the centrifugal force felt by fluid elements. Rotating disk flows are one of three classes of 3DTBLs. The other classes are pressure-driven flows such as the flow on the endwall of a bend or around an obstacle and shear-driven flows which occur when a wall moves in a direction different from the main flow direction. These classes of 3DTBLs generally begin as 2DTBLs and are perturbed into three dimensions by the pressure gradient or wall shear. Thus, they are expected to have strongly non-equilibrium characteristics. The disk boundary layer is unique because it maintains nearly constant skewing all the way from its origin as a laminar boundary layer through its development as a turbulent boundary layer. Thus, the disk boundary layer provides the opportunity to study turbulence in equilibrium with a skewed mean velocity profile.

Two common characteristics differentiate 3DTBLs from 2DTBLs: (i) the shear stress vector is misaligned from the mean strain rate vector and (ii) there is a reduction in the turbulence's ability to mix momentum for a given amount of turbulent kinetic energy. The latter is normally described using the $a_1$ parameter, $a_1 = -\overline{u'v'}/k^2$

($k^2$ is twice the turbulent kinetic energy), a parameter used to calculate the $c_\mu$ constant important in the $\kappa$–$\varepsilon$ equation set. The $a_1$ parameter is consistently 0.15 in 2DTBLs but can be much lower in 3DTBLs. Recent studies have focused on structural features of the turbulence in an effort to explain reduced shear stress levels observed in previous 3DTBL experiments. Littell & Eaton (1991) measured single-point and two-point statistics in an air-flow disk apparatus, and Chiang & Eaton (1993) made a flow visualization study of the near-wall structure in a water-flow apparatus. These studies led to the conclusion that gradients in the cross-flow velocity profile render the near-wall structures less efficient at producing sweeps and bursts, the two events associated with large shear stress production in turbulent boundary layers. Fleming & Simpson (1994) examined the near-wall streaky structures in two- and three-dimensional boundary layers using hydrogen bubble flow visualization. They found that structures in the three-dimensional flow are more stable and quiescent while the streaks in the two-dimensional flow oscillate energetically and interact more with the surrounding fluid.

Johnston & Flack (1996) compared 11 recent 3DTBL experiments and concluded that the stronger the cross-stream pressure gradient, the more skewing there is in the inner layer and the larger the reduction in $a_1$. Their hydrogen bubble flow visualization of the sublayer and buffer regions in two 3DTBLs showed that the strength of ejections did not change with cross-stream pressure gradient, but the frequency of the ejection events did.

The same turbulent eddies responsible for shear stress production are often associated with heat flux production. Perry & Hoffmann (1976) showed a high probability of coincidence between strong momentum and heat flux events in their study of a heated 2DTBL. This leads to the hypothesis that the turbulent heat flux in 3DTBLs will be lower than predicted by conventional models. What is not clear, though, is which will be affected more by the skewing, the turbulent shear stress or the turbulent heat flux. Of particular interest to modellers is the turbulent Prandtl number which indicates the relative strengths of turbulent mixing of heat and momentum.

The rotating disk flow has been studied extensively (see review in Littell & Eaton 1991) including several studies of the surface heat transfer from an isothermal surface (Cobb & Saunders 1956; Popiel & Boguslawski 1975; and McComas & Hartnett 1970). Elkins & Eaton (1994) measured the heat transfer from a uniform heat flux surface while Tadros & Erian (1983) computed the heat transfer for both isothermal and uniform heat flux conditions. There have been no reported measurements of the turbulent heat flux or other scalar transport in disk flows, nor have there been turbulent heat transport measurements reported for other simple 3DTBLs. Abrahamson & Eaton (1991) investigated the effect that three-dimensionality has on turbulent heat transfer by measuring the surface heat transfer coefficients from a uniform heat flux surface in the flow around a 60° and a 90° wedge. The results showed that an increase in the three-dimensionality of the flow reduced the surface heat transfer rate. Their measurements provided little insight into why or how the turbulent heat transfer is decreased.

The objectives of this experiment were to measure all of the turbulent heat flux components and to calculate the turbulent Prandtl number for the disk flow. These data will be useful for heat transfer modelling, but more importantly, they provide an additional avenue to explore turbulence structure modification by mean flow skewing. Heated two-dimensional turbulent boundary layer cases are well-documented in the experiments of Antonia, Danh & Prabhu (1977), Subramanian & Antonia (1981), Gibson & Verriopoulos (1984), and many others. The effects of the three-

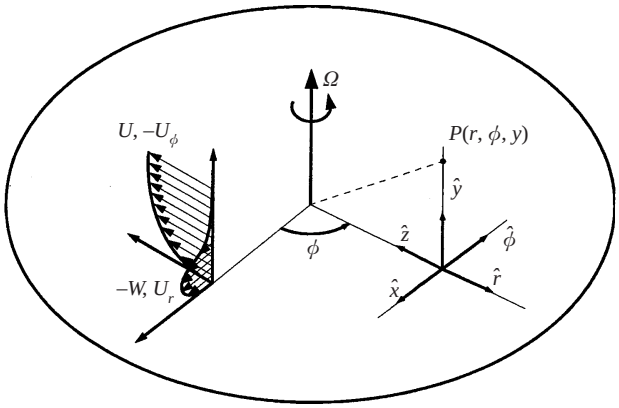


FIGURE 1. Mean tangential and radial velocity profiles in the rotating disk boundary layer as seen in the rotating reference frame. Also shown are the coordinate systems used in this study.

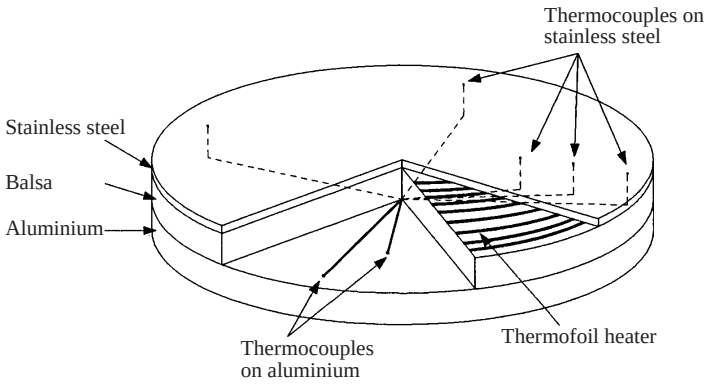


FIGURE 2. Construction of the heat transfer disk.

dimensionality in the rotating disk boundary layer will be evaluated by comparing the results of the present experiment to these 2DTBL data.

## 2. Facility and experimental techniques

The experiment used the apparatus of Littell & Eaton (1991) modified for heat transfer studies. A 1 m diameter heated disk with a nominally uniform surface heat flux rotated in still air with a vertical axis of rotation. The disk (see figure 2) had a composite construction with a 13 mm thick aluminium base disk, a 13 mm thick insulating layer of balsa wood, a thermofoil heater supplying an approximately uniform heat flux up to $1\,\mathrm{kW\,m^{-2}}$, and a 1 mm thick layer of stainless steel which served as the surface for the boundary layer. Because of the composite construction of the disk, the surface was slightly wavy with a maximum variation of $\pm 0.15$ mm. The height variation did not measurably affect the turbulence as is evident in the agreement between present results and the measurements of Littell & Eaton (1991) who used a much flatter disk. However, it was necessary to phase lock the data sampling to the disk rotation when the probes were close to the disk where vertical gradients in the boundary layer were steep. In these cases, measurements were taken only when a specific 6° sector of the disk passed below the probes. The maximum

rotation speed was 1000 r.p.m. which gave a maximum Reynolds number of $10^6$ at a 40 cm radius, the primary measurement location.

The thermofoil heater was split into three different annular regions. The central portion with a 7.5 cm radius was unheated. The region from 7.5 cm to 20 cm radius was heated by an inner heater and from 20 cm to 48 cm by an outer heater. Two different boundary conditions were investigated using this system: BC1 had a uniform heat flux surface for radii from 7.5 cm to 48 cm, and BC2 had a uniform heat flux surface over the annular region for radii from 20 cm to 48 cm. The first boundary condition heated the region of the disk with laminar, transitional, and turbulent flow while the second heated only the turbulent region.

A 30 cm wide annular apron surrounding the disk was used to separate the boundary layers on the top and bottom surfaces of the disk. Vanes were mounted on the top surface of the apron to turn the flow coming off of the disk. This removed the angular momentum of the exiting boundary layer to provide a quiescent entrainment flow in the 2.4 m wide by 2.7 m deep by 3.0 m tall test cell. The effectiveness of these vanes is confirmed by the excellent agreement between the measured velocity field and the analytic solution for laminar flow on a rotating disk in an infinite, quiescent medium. The bottom of the disk was completely enclosed by an insulated, temperature-controlled shroud to eliminate fluid dynamic disturbances caused by the bottom side boundary layer and to minimize the backloss of heat. For each Reynolds number, the rig was run until the surface temperature distribution reached steady state. By controlling the shroud temperature, the temperature differences between the disk and the ambient air drifted less than 0.1 °C over the entire data taking period which lasted for 1–2 hours.

The probe traverse was mounted 1 m above the disk on a steel arch that was vibrationally isolated from the support frame. Translational resolution in the vertical direction was 1.6 μm and rotational resolution about the probe stem was 0.5°.

Constant-temperature thermal anemometers (TSI Model IFA-100) were used to measure velocity, and a custom constant-current anemometer was used to measure temperature. It was estimated from a power spectrum of the tangential velocity fluctuations that a 3 kHz bandwidth was necessary for the probes to capture the energy-containing scales in the flow. A digital compensation technique based on the method of Wroblewski & Eibeck (1990) was used to extend the frequency response of the cold wires up to 3 kHz.

In this method, a wire transfer function is calculated in the frequency domain from theory using the calibrated time constants of the probe prongs, wire plating, and the active region of the cold wire. The temperature signal is filtered at 10 kHz using a low-pass 8-pole Butterworth filter and sampled at 20 kHz. Each data record is fast Fourier transformed, divided by the wire transfer function, and then inverse fast Fourier transformed to reconstruct the actual temperature time record. More details are available in Elkins & Eaton (1997).

Three probes were used in the experiment: the dual-wire probe of Littell & Eaton (1991) was used to measure the mean velocity and temperature, a single cold wire was used to measure mean and fluctuating temperature, and a custom three-wire heat flux probe (see figure 3) was used to measure the Reynolds stresses and the turbulent heat fluxes. The dual-wire probe used two 5 μm diameter platinum-coated tungsten wires with $l/d = 270$ lying in a plane parallel to the disk surface but oriented at $\pm 45°$ to the probe axis. Using $l/d > 250$ ensured the cosine law could be used for these wires. Details of the use of this probe for measurements in the heated boundary layer are found in Elkins & Eaton (1997).

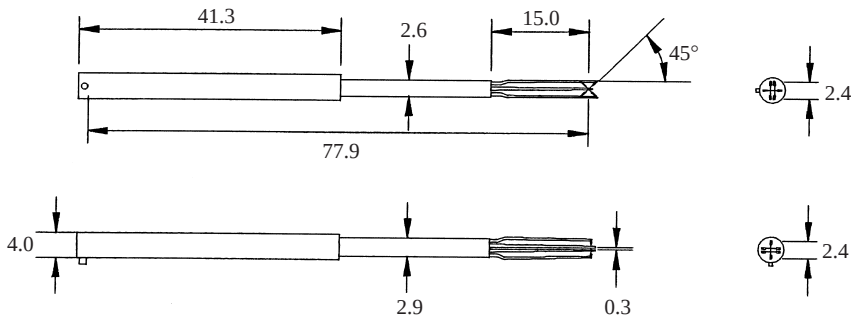


FIGURE 3. Triple-wire heat flux probe used to measure Reynolds stresses and heat fluxes. Dimensions in mm.

The single cold-wire probe was made with 1 μm Pt–10%Rh Wollaston wire. A large $l/d = 900$ was used to decrease the effects of the wire plating and probe prongs in order to simplify the frequency compensation for the 1 μm probe. An operating current of 0.2 mA was used which resulted in self-heating of less than 0.1 °C for velocities greater than 1 m s$^{-1}$. This probe was used to take turbulent temperature measurements close to the disk.

The three-wire heat flux probe consisted of two 2.5 μm platinum-coated tungsten hot wires separated by 0.35 mm in a cross-wire formation with a 2.5 μm cold wire placed 0.55 mm upstream of the geometric centre of the cross-wire and perpendicular to the plane of measurement of the cross-wire. The size parameters were chosen following design criteria given in the literature (Wyngaard 1968; Guitton & Patel 1969; Gessner & Moller 1971; Strohl & Comte-Bellot 1973; Nakayama & Westphal 1986; Blair & Bennett 1987; Ligrani & Bradshaw 1987*a*, *b*) and following a similar design to that used by Littell & Eaton for their cross-wires. This was done to achieve the best resolution while still measuring temperature and velocity without interference effects. This probe could be oriented in four different roll positions each separated by 45° in order to measure all Reynolds stress and turbulent heat flux components. The current used for the 2.5 μm cold wire was 1 mA which produced an overheat of 0.3 °C at 1 m s$^{-1}$. Since the 2.5 μm cold wire measured temperature fluctuations which are not as sensitive to overheat, mean temperature accuracy was sacrificed for a higher signal-to-noise ratio.

The probe signals were conditioned with Frequency Devices model 901F1 low-pass 8-pole Butterworth filters with cutoff frequencies of 10 kHz. The signals were sampled using a MSE 386 pc clone, a Metrabyte DAS-20 12 bit A/D board, and a SSH-4 simultaneous sample and hold card.

Because of the size of this probe, measurements could be taken only as close as $y/\delta_2 = 1.1$, $y^+ = 123$ for $Re = 6.5 \times 10^5$ and $y/\delta_2 = 1.2$, $y^+ = 193$ for $Re = 10^6$. Above these heights, the features of the disk height profile were washed out so it was not necessary to phase lock the measurements. As the probes were in the stationary lab frame, the thermal wake from the hot wires contaminated the cold-wire temperature signal at heights very far from the disk where the percentage of turbulent flow, intermittency, was less than 80%. This made heat flux measurements impossible at heights above $y/\delta_2 = 5.8$, $y^+ = 650$ for $Re = 6.5 \times 10^5$ and $y/\delta_2 = 7.2$, $y^+ = 1210$ for $Re = 10^6$.

The experimental uncertainties are listed in table 1. Uncertainty for the mean velocity and Reynolds stresses match those of Littell & Eaton since similar measure-

| Quantity | Uncertainty | % of Quantity |
|---|---|---|
| $\overline{U}$ | 3% | $\overline{U}$ |
| $\overline{u'^2}$ | 5% | $\overline{u'^2}$ |
| $\overline{v'^2}$ | 5% | $\overline{u'^2}$ |
| $\overline{w'^2}$ | 5% | $\overline{u'^2}$ |
| $\overline{u'v'}$ | 10% | $\overline{u'v'}$ |
| $\overline{v'w'}$ | 15% | $\overline{u'v'}$ |
| $\overline{u'w'}$ | 10% | $\overline{u'v'}$ |
| $\overline{T} - T_\infty$ | 5% | $\overline{T} - T_\infty$ |
| $\overline{\theta'^2}$, 1 μm | 5% | $\overline{\theta'^2}$ |
| $\overline{\theta'^2}$, 2.5 μm | 15% | $\overline{\theta'^2}$ |
| $\overline{u'\theta'}$ | 11% | $\overline{u'\theta'}$ |
| $\overline{v'\theta'}$ | 11% | $\overline{v'\theta'}$ |
| $\overline{w'\theta'}$ | 12% | $\overline{w'\theta'}$ |
| $Pr_t$ | 17% | $Pr_t$ |

TABLE 1. Uncertainties in the quantities measured with the 1 μm single cold wire and the heat flux probe. Cross-wire uncertainties from Anderson & Eaton (1989).

ment techniques were employed in this study. The frequency compensation of the temperature signal accounts for most of the uncertainty in the turbulent heat flux quantities. The uncertainty for these quantities was estimated from the analysis of Wroblewski & Eibeck (1990) since the frequency compensation in this study is based on their methods. Using these estimates, the uncertainty for $Pr_t$ is 17% for the data closest to the disk and is due mainly to uncertainty in $\overline{v'\theta'}$. As discussed by Littell & Eaton (1994), the uncertainty in the measured quantities is expected to increase with distance from the disk as the turbulence intensity increases. In their conservative estimates, the uncertainty doubles for a turbulence intensity of 40% corresponding to a height of $y/\delta_2 \approx 5$.

There is another contribution to uncertainty that was not considered in the above analyses: the effects of wire length and wire spacing. Although the heat flux probe was designed using criteria documented in the literature, it is believed that the probe under-measures turbulent velocities, especially $v'$. In previous 2DTBL studies such as Blair & Bennett (1987), a correction for the effects of wire spacing was applied. However, there is some question as to what an appropriate correction would be in a 3DTBL, so no correction was applied in this study. Since it is primarily a problem in $v'$, both $u'v'$ and $v'\theta'$ are affected similarly, and the overall effect on $Pr_t$ cancels to some extent. Conservative estimates of this error add 4% to the previously stated uncertainty of $Pr_t$ for $y/\delta_2 \approx 1$, but this uncertainty decreases with probe height as the measurement of $v'$ becomes more absolutely accurate in the outer layer. It should be stated that although the absolute values of the $u'$, $v'$, and $w'$ dependent quantities may have high uncertainties, the general trends in the data, i.e. the differences and similarities between BC1 and BC2 for both Reynolds numbers, are believed to be real and significant.

## 3. Results

### 3.1. *Mean velocity*

The results are presented in the disk frame of reference which is right-handed and has its origin at the measurement radius. For convenience in comparing these

| $Re$ at $r = 0.4$ m | Boundary condition | $U_{disk}$ (m s$^{-1}$) | $\delta_1$ (mm) | $\delta_2$ (mm) | $Re_{\delta_2}$ | $\delta_H$ (mm) | $T_\tau$ (°C) | $u_\tau$ (m s$^{-1}$) | $\nu/u_\tau$ (μm) | $T_{disk} - T_\infty$ (°C) |
|---|---|---|---|---|---|---|---|---|---|---|
| $6.5 \times 10^5$ | BC1 | 25.26 | 2.27 | 1.62 | 2480 | 3.67 | 0.38 | 1.13 | 14.6 | 10.3 |
| $6.5 \times 10^5$ | BC2 | 25.26 | 2.24 | 1.63 | 2480 | 2.98 | 0.41 | 1.13 | 14.7 | 10.2 |
| $10^6$ | BC1 | 42.10 | 2.13 | 1.56 | 3970 | 3.21 | 0.33 | 1.79 | 9.3 | 9.6 |
| $10^6$ | BC2 | 42.10 | 2.13 | 1.56 | 3970 | 2.80 | 0.39 | 1.78 | 9.3 | 10.8 |

TABLE 2. Summary of boundary layer parameters for the four turbulent cases.

results with other studies, the cylindrical coordinates and velocities are redefined in terms of Cartesian coordinates and velocities (Figure 1). In this frame of reference, the $+y$-direction is vertically upward, the $+x$-coordinate is in the negative tangential direction, and the $+z$-coordinate is in the negative radial direction pointing at the axis of rotation. The velocities $V$, $U$, and $W$ correspond to these coordinates, respectively. These velocities are defined with respect to velocities in cylindrical coordinates as

$$(-W, -U, V) = (U_r, U_\phi, U_y).$$

Note that the negative signs result from the definition that positive $U$ in the rotating frame results from positive rotation $\Omega$.

In the lab frame, the velocity at the edge of the boundary layer is zero which makes it difficult to determine $\delta_{99}$. An alternative boundary layer length scale is provided by the momentum thickness based on the velocity vector magnitude, denoted by $\delta_2$. This quantity is determined with better certainty in the disk flow and will be used to normalize most of the results that follow. Other integral parameters as well as the operating conditions for the two Reynolds numbers, $6.5 \times 10^5$ and $10^6$ and both boundary conditions are listed in table 2.

Figure 4 compares the total velocity magnitude in the disk frame from the present experiment with BC1 to Littell & Eaton's (1991) results. The cross-flow velocity profiles are shown in figure 5. Similar profiles were obtained in the BC2 cases. The close agreement between the heated and unheated mean flow and Reynolds stresses as will be shown below indicates that the physics in the momentum boundary layer is not altered by the heating.

Littell showed that with an appropriate choice of skin friction coefficient, the mean tangential velocity can be fit by the conventional log law with constants $\kappa = 0.41$ and $C = 5.0$. Figure 6 compares the mean tangential velocity profile in a semi-log plot with the log law including the Van Driest model for the buffer region. Values for $u_\tau$ were alternatively calculated by fitting the mean temperature data to the conventional thermal log law (see (3.3)). While there is some question as to whether the conventional flat-plate log laws apply in this three-dimensional flow, the values for $u_\tau$ determined by each method agree to within a few percent justifying the use of $u_\tau$ as an internally consistent velocity scale in the results that follow.

One noteworthy characteristic of the mean velocity profiles is the lack of a wake profile. Littell associated this with the acceleration of the boundary layer as it moves to larger radii. In the disk flow, the tangential velocity increases proportionally with radius, and the effect of this on the mean velocity profile is similar to the acceleration created by favourable pressure gradients in 2DTBLs (cf. Blair 1981). In the outer layer, the large eddies circulate fluid which has come from slower radii, creating the slightly lower mean velocities in the wake region of figure 6.

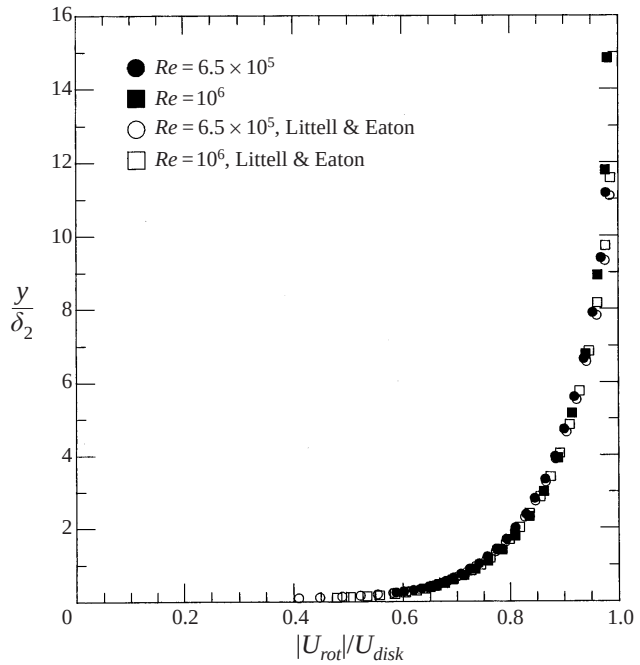


FIGURE 4. Mean velocity vector magnitude in the rotating frame for turbulent flow with $Re = 6.5 \times 10^5$ and $10^6$, $r = 0.4$ m. Results from Littell & Eaton (1991) are provided for comparison.

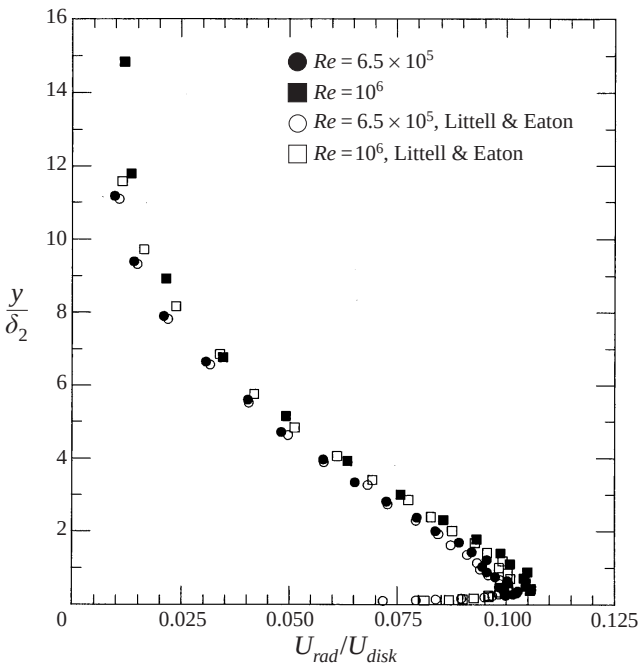


FIGURE 5. Radial mean velocity for turbulent flow with $Re = 6.5 \times 10^5$ and $10^6$. Results from Littell & Eaton (1991) are provided for comparison.

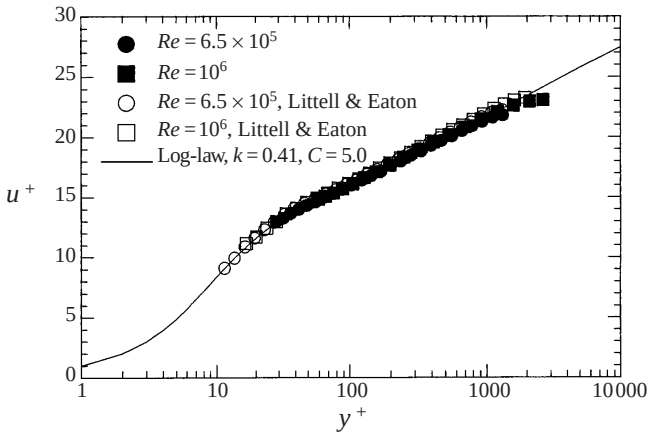


FIGURE 6. Mean tangential velocity in the rotating frame plotted in wall coordinates for $Re = 6.5 \times 10^5$ and $10^6$. Results from Littell & Eaton (1991) are provided for comparison.

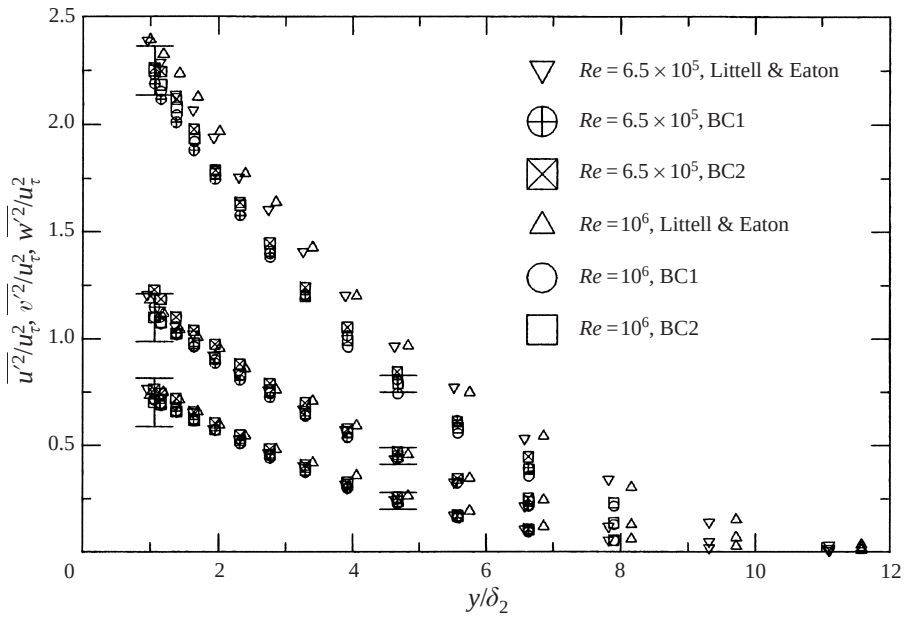


FIGURE 7. Normal Reynolds stresses $\overline{u'^2}/u_\tau^2$ (or $\overline{u_\phi'^2}/u_\tau^2$), $\overline{v'^2}/u_\tau^2$ (or $\overline{u_y'^2}/u_\tau^2$), and $\overline{w'^2}/u_\tau^2$ (or $\overline{u_r'^2}/u_\tau^2$) vs. $y/\delta_2$ for $Re = 6.5 \times 10^5$ and $10^6$, $r = 0.4$ m. Error bars from table 1.

### 3.2. *Turbulent velocity characteristics*

The three Reynolds normal stresses measured in the heated boundary layer are shown in figure 7. The normal stress ratios are similar to other two- and three-dimensional boundary layers in that $\overline{u'^2} \approx 2\overline{w'^2} \approx 3\overline{v'^2}$. The agreement with Littell is quite good except for a discrepancy in $\overline{u'^2}/u_\tau^2$ which is 5% lower than Littell's results near the wall. Repeating the measurements for an isothermal case gave the same result as the heated case indicating that the small discrepancy in $\overline{u'^2}$ is related to physical characteristics of the heat transfer disk.

The results for the three Reynolds shear stresses are shown in figures 8(*a*), 8(*b*), and

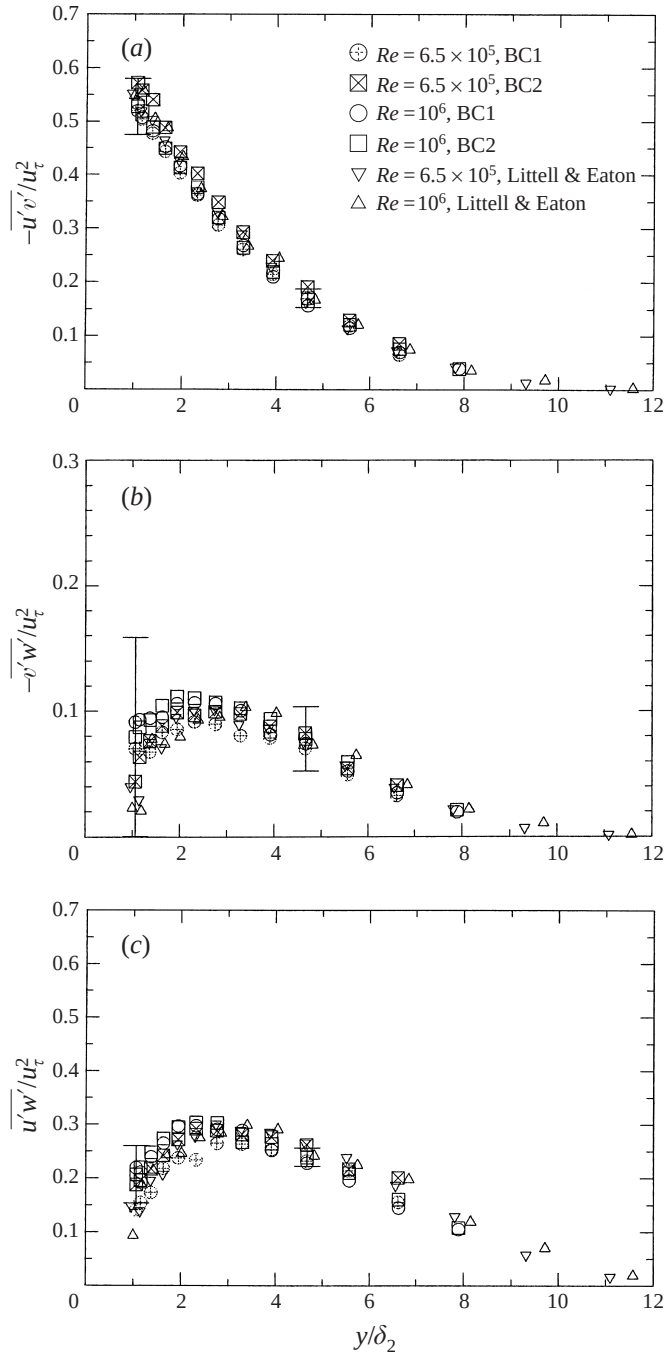


FIGURE 8. Reynolds shear stresses: (*a*) $-\overline{u'v'}/u_\tau^2$ (or $\overline{u'_\phi u'_y}/u_\tau^2$), (*b*) $-\overline{v'w'}/u_\tau^2$ (or $\overline{u'_y u'_r}/u_\tau^2$), and (*c*) $\overline{u'w'}/u_\tau^2$ (or $\overline{u'_\phi u'_r}/u_\tau^2$), all vs. $y/\delta_2$ for $Re = 6.5 \times 10^5$ and $10^6$, $r = 0.4$ m. Error bars from table 1.

8(*c*). The presence of the cross-flow results in the two stresses $-\rho\overline{v'w'}$ and $\rho\overline{u'w'}$ which are zero in 2DBLs. The profile for $-\overline{v'w'}$ shows that it reaches a peak and then turns toward zero around $y/\delta_2 = 2$. This profile should cross zero around $y/\delta_2 = 0.5$ which corresponds to the location where the mean radial shear rate, $\partial\overline{W}/\partial y$, changes sign.

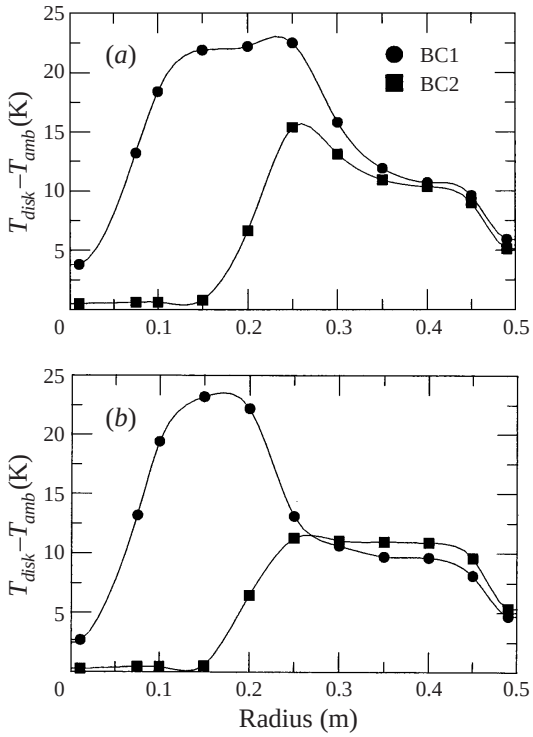


FIGURE 9. Radial surface temperature profiles for (*a*) $Re = 6.5 \times 10^5$ and (*b*) $Re = 10^6$ for BC1 and BC2. In these profiles, the curves are cubic splines fit to the thermocouple measurements represented by the symbols. The primary measurement location is $r = 0.4$ m.

The primary shear stress component, $-\rho\overline{u'v'}$, differs significantly from its values in 2DTBLs. Subramanian & Antonia (1981) show that $-\overline{u'v'}/u_\tau^2$ is nearly constant and slightly less than 1 at $y/\delta_2 \approx 1$, and the value decreases linearly to zero at the edge of the boundary layer. The present measurements show lower levels of shear stress and a different profile shape in which $\overline{u'v'}$ decreases rapidly from the wall value and asymptotes to zero giving a concave-up shape. The differences can be explained by integral momentum balances. In the turbulent flat-plate boundary layer with no pressure gradient, the wall shear stress is balanced by viscous shear, $\rho\overline{u'v'}$, and a streamwise change in momentum as the boundary layer grows. A conservation of angular momentum analysis in the disk boundary layer shows that an additional radial flux term changes the shear stress characteristics. Estimates made from an integral analysis using mean flow measurements indicate $-\overline{u'v'}/u_\tau^2$ should reach a maximum value between 0.8 and 0.9 for $y/\delta_2 < 1$. In figure 8(*a*), the value of $-\overline{u'v'}/u_\tau^2$ is 0.5 at $y/\delta_2 = 1$. Part of the reason this value is low is the difficulty in measuring $v'$ discussed in § 2. The uncertainty in $u_\tau$ already discussed may also contribute to this deviation.

### 3.3. *Mean temperature*

The heat transfer coefficient in the rotating disk boundary layer is constant with radius in laminar flow, increases rapidly with radius through the transition region ($h \propto r^7$), and increases slowly with radius in the turbulent flow ($h \propto r^{0.6}$). For the uniform surface heat flux boundary condition, this creates a surface temperature profile with a mildly negative radial temperature gradient at the measurement location of $r = 40$ cm

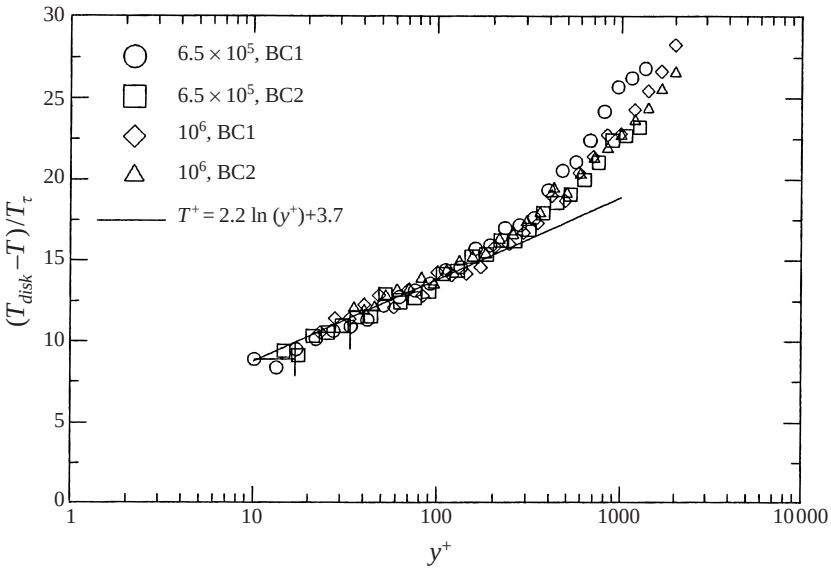


FIGURE 10. Mean temperature difference measured with the 1 μm diameter cold wire plotted in wall coordinates for $Re = 6.5 \times 10^5$ and $10^6$ for BC1 and BC2, $r = 0.4$ m. The error bars indicate uncertainty range for the probe position.

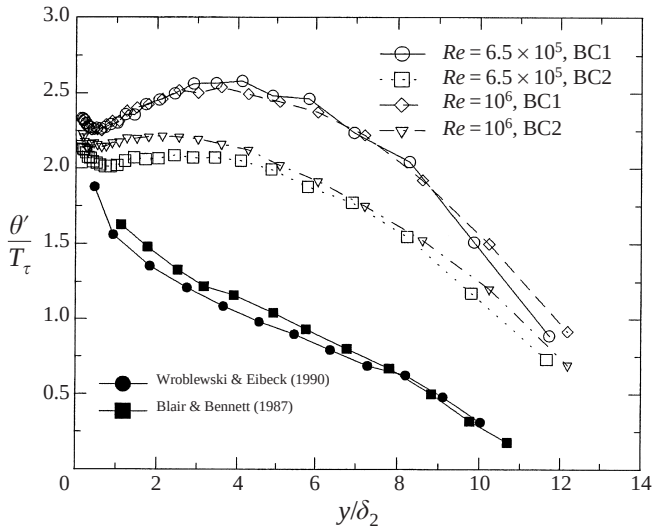


FIGURE 11. 1 μm cold wire results for $(\overline{\theta'^2})^{1/2}$ normalized by the friction temperature for $Re = 6.5 \times 10^5$ and $10^6$ for BC1 and BC2, $r = 0.4$ m. Measurements made in a 2DBL by Wroblewski & Eibeck (1990) and Blair & Bennett (1987) are shown for comparison.

for both Reynolds numbers and boundary conditions studied. The surface temperature profiles for $Re = 6.5 \times 10^5$ and $10^6$ are shown in figures 9(*a*) and 9(*b*), respectively.

Volino & Simon (1994) have shown that the thermal law of the wall is very sensitive to streamwise accelerations due to pressure gradients for 2DTBL flow. Although the disk flow experiences acceleration, agreement with the traditional thermal law of the wall ($\kappa_\theta = 0.46$ and $C_\theta = 3.6$, Kays & Crawford 1980) is fairly good. The data shown in figure 10 are normalized using different values for $u_\tau$ than those in table 2. These

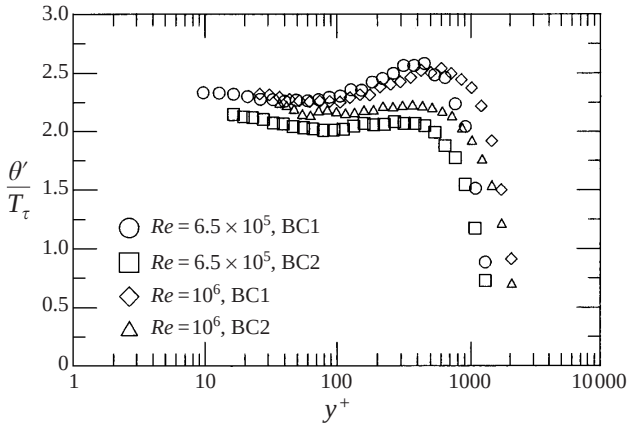


FIGURE 12. 1 μm cold wire results for $(\overline{\theta'^2})^{1/2}$ normalized by the friction temperature and plotted in semi-log coordinates for $Re = 6.5 \times 10^5$ and $10^6$ for BC1 and BC2.

values are lower by 3–5% except in the $Re = 6.5 \times 10^5$ BC1 case in which $u_\tau$ is 5% higher. There is an uncertainty of 100 μm in the probe height due to changes in the disk height and circumferential surface profile as the disk was heated to steady state. The profiles have been offset by this amount and the uncertainty for each Reynolds number is shown in figure 10 by the error bars at the inner most points.

Surprisingly, above $y^+ = 300$, there are wake profiles in the temperature data while the wake profiles were absent in the velocity data. These profiles show a significant dependence on upstream boundary condition. The BC1 profiles have higher values than their respective BC2 profiles at the outer edge of the boundary layer since the development lengths for the thermal boundary layer are greater.

### 3.4. *Temperature fluctuations*

Figure 11 shows 1 μm cold wire measurements of the turbulent temperature fluctuations, $\theta'$, compared to two 2DTBLs (Wroblewski & Eibeck 1990, $Re_{\delta_2} = 3300$ and Blair & Bennett 1987, $Re_{\delta_2} = 5400$). $T_\tau\,(q_w/(\rho c_p u_\tau))$ provides the best temperature scale for these data. To be consistent, the normal coordinate is scaled by $\delta_2$; however, $\delta_H$

$$\int_0^\infty \frac{U_{tot}}{U_{disk}} \left( \frac{T - T_\infty}{T_{disk} - T_\infty} \right) \mathrm{d}y$$

does a better job of scaling the temperature fluctuation data by aligning the outer layer peaks. Close to the disk there is a peak of about the same magnitude as found in 2DTBLs, but there is an additional peak in the outer layer that will be discussed below.

Figure 12 shows a semi-log plot of $\theta'$ in inner coordinates demonstrating that the peak in $\theta'$ occurs between $y^+ = 300$ and 400, at the start of the wake region in the mean temperature profile. The surface temperatures are high in the laminar region at small radii, and much lower in the transition and turbulent regions. It is hypothesized that fluid that is warmed passing over the laminar region is rolled up into the large eddies of the transition and turbulent regions. This fluid remains warm for a significant distance downstream due to weak turbulent diffusivity in the outer layer. The large eddies mix the hot fluid from far upstream and relatively cool fluid from nearby causing high values for the turbulent temperature fluctuations. The

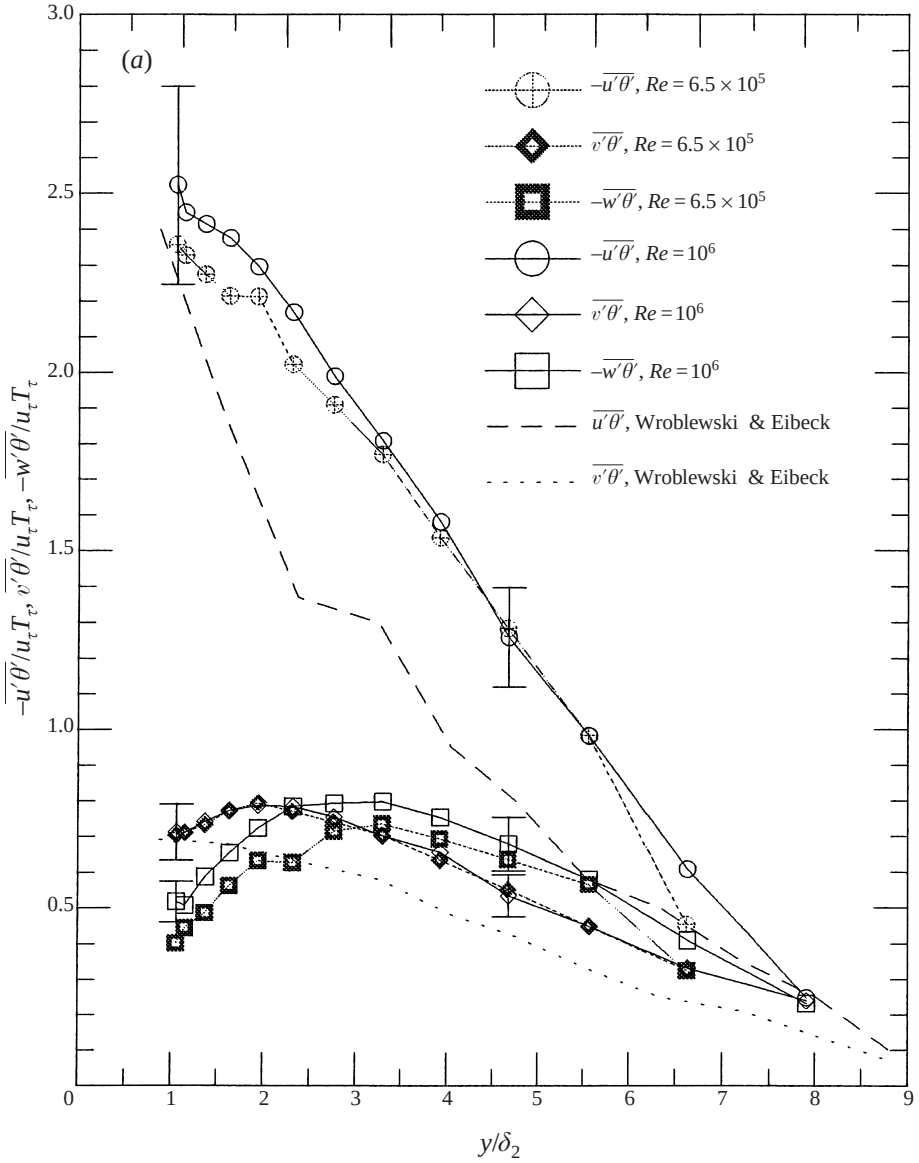


FIGURE 13(*a*). For caption see facing page.

presence of hot fluid also helps explain the boundary condition dependence of the wake profiles in the mean temperature data.

There are a few clues which confirm this hypothesis. The first is that the data for BC1 have the largest $\theta'$ peaks and the highest temperatures in the laminar and transition regions. The second is that the peaks move out for the higher Reynolds number cases. This suggests that the warm fluid is slowly being pushed out with boundary layer development. A final clue is that there is no production peak for $\theta'$ in the outer portion of the boundary layer. Since $\theta'$ must come from somewhere, it is likely that it is created upstream. G. N. Coleman (1997, personal communication) observed a similar outer layer peak in his simulation of a heated, incompressible Ekman layer and suggested that it was created early and was diffusing outward

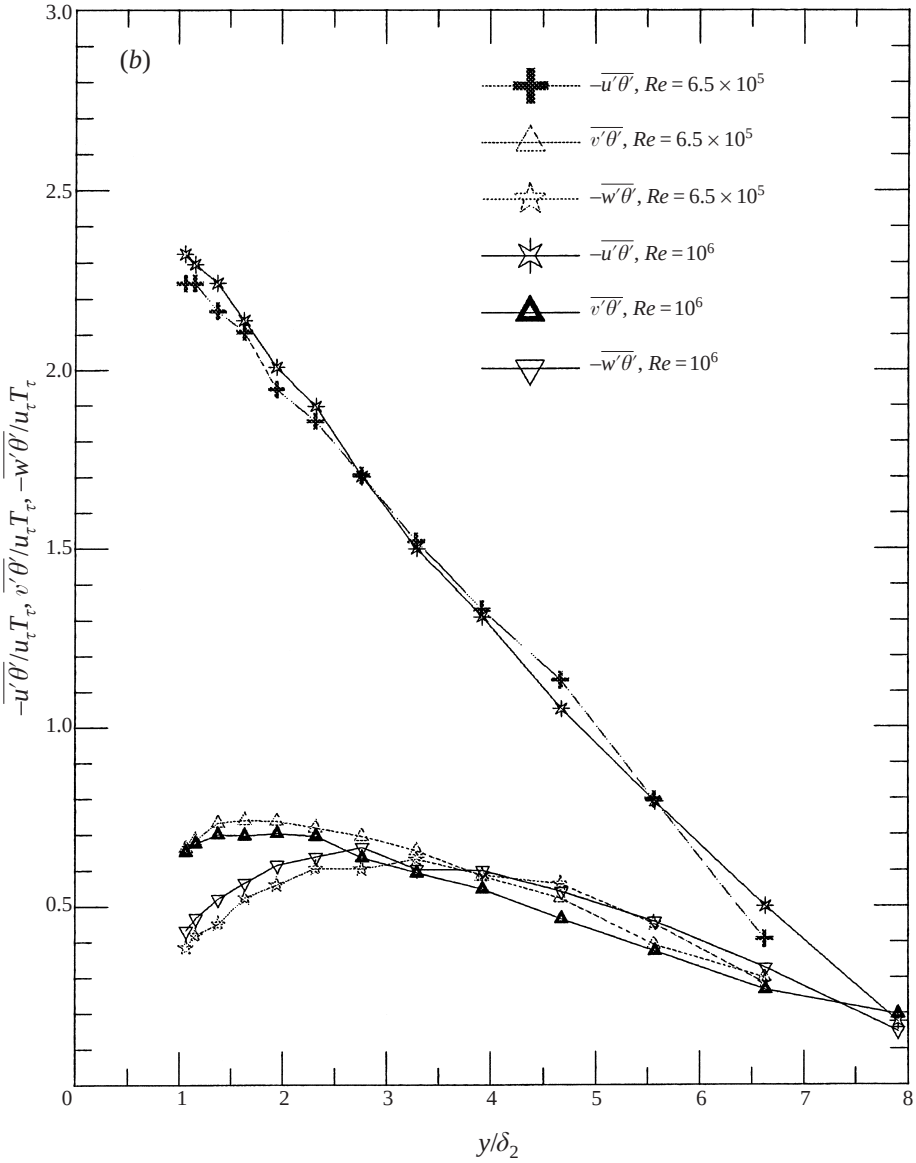


FIGURE 13. (*a*) The turbulent heat fluxes $-\overline{u'\theta'}$, $\overline{v'\theta'}$, and $-\overline{w'\theta'}$ for $Re = 6.5 \times 10^5$ and $10^6$ with BC1 compared to $\overline{u'\theta'}$ and $\overline{v'\theta'}$ measured by Wroblewski & Eibeck (1990) in a 2D flat plate boundary layer. Error bars indicate uncertainty from table 1. (*b*) As (*a*) but for BC2.

with time. It is hypothesized that at very high Reynolds numbers, the $\theta'$ profiles will appear more like the profile for BC2 and $Re = 10^6$ since only the slight negative radial temperature gradient will be driving the levels of $\theta'$ in the outer layer.

### 3.5. *Turbulent heat fluxes*

Figure 13(*a*) compares the turbulent heat flux measurements for BC1 to typical values for the heat fluxes in a 2DBL, and figure 13(*b*) shows the same measurements for BC2. A significant difference between the disk and flat plate is the existence of the cross-stream heat flux $-\overline{w'\theta'}$ which is zero for 2DBLs. The $-\overline{u'\theta'}$ and $\overline{v'\theta'}$

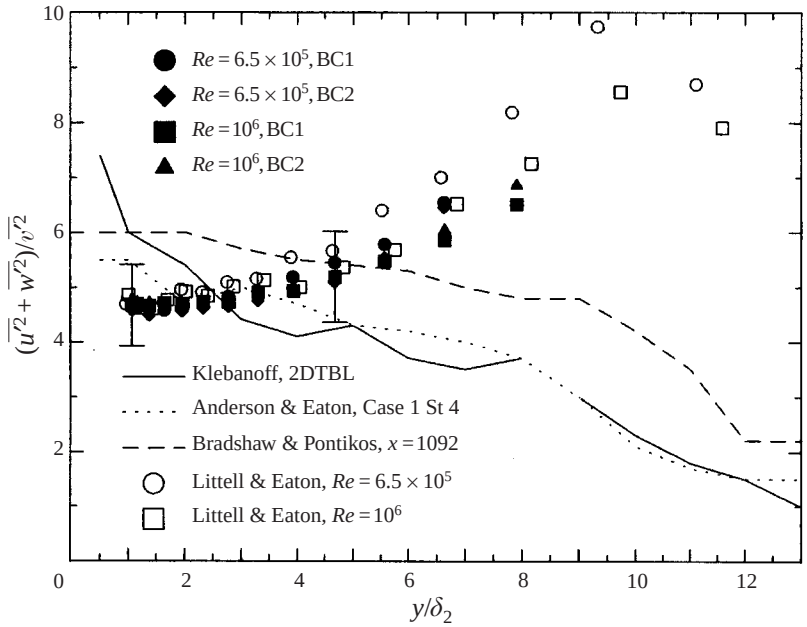


FIGURE 14. The structure parameter $(\overline{u'^2} + \overline{w'^2})/\overline{v'^2}$ for all cases. Error bars from table 1.

profiles agree much better than the profiles for the radial heat fluxes, which show large differences between Reynolds numbers and boundary conditions. The values of $\overline{v'\theta'}/u_\tau T_\tau$ at points closest to the disk are well below a value of 1 suggested by integral analysis. As discussed in § 2, this is primarily due to difficulty in measuring $v'$ with the cross-wire. Although the values are low, the measurements should be self-consistent, and the differences observed between cases are believed to be real.

Normalization by enthalpy thickness does a fair job of collapsing the data for $-\overline{u'\theta'}$ and $\overline{v'\theta'}$, and, in particular, aligns the peaks in the $\overline{v'\theta'}$ and $-\overline{w'\theta'}$ fluxes. The peaks for $\overline{v'\theta'}$ occur around $y/\delta_H = 1$, and the peaks for $\overline{w'\theta'}$ occur at $y/\delta_H = 1.5$. Interestingly, the peaks for $\theta'$ occurred around $y/\delta_H = 1.5$–2. Also worth noting is that the radial heat fluxes in the outer layer are largest in the BC1 cases which had the largest $\theta'$ peak values. This suggests a stronger relationship between the radial heat flux and the temperature fluctuations than for the other two turbulent heat flux quantities.

### 3.6. *Structure parameters*

Correlation coefficients and structural parameters often are at the heart of single-point turbulence models. One hopes that these parameters are less sensitive to flow geometry than the turbulent stresses and heat fluxes.

Figure 14 shows the ratio of the wall-parallel normal stresses to the vertical normal stress,

$$\frac{\overline{u'^2} + \overline{w'^2}}{\overline{v'^2}}.$$

This parameter is a measure of the coherence of the turbulent structures. The behaviour of this ratio is very different from its behaviour in 2DBLs (Klebanoff 1954) and 3DTBLs (Bradshaw & Pontikos 1985; Anderson & Eaton 1989). In other flows,

the parameter starts high with a value between 5 and 8 near the wall and then monotonically decreases to around 2 at the outer edge of the boundary layer. In the disk flow, the parameter starts low and increases before peaking in the outer layer showing that the vertical motion is strong close to the disk but decreases relative to the streamwise motion in the outer part of the flow.

The $a_1$ parameter, defined for the disk flow as the ratio of the vector magnitude of the shear stress to twice the turbulent kinetic energy,

$$a_1 = \frac{\left(\overline{u'v'}^2 + \overline{v'w'}^2\right)^{1/2}}{k^2},$$

represents the amount of turbulent mixing of momentum for a given level of turbulence. Similar to other 3DBLs, the parameter is smaller than in 2DBLs indicating that the disk boundary layer is less effective at creating shear stress from turbulent motion. The reader is referred to Littell & Eaton (1991) for a detailed comparison of $a_1$ to other 3DBL results.

The correlation coefficients $R_{u\theta}$ and $R_{v\theta}$ are defined, respectively, as

$$R_{u\theta} = \frac{\left(\overline{u'\theta'}^2 + \overline{w'\theta'}^2\right)^{1/2}}{\theta'\left(\overline{u'^2} + \overline{w'^2}\right)^{1/2}} \quad \text{and} \quad R_{v\theta} = \frac{\overline{v'\theta'}}{\theta'\left(\overline{v'^2}\right)^{1/2}}.$$

In 2DTBLs, $R_{u\theta}$ is normally constant and approximately 0.7–0.8 while $R_{v\theta}$ is constant as well and approximately 0.40–0.45. Figure 15(*a*) shows that there is a region where $R_{u\theta} \approx 0.5$ below $y/\delta_2 \approx 4$ but then the profiles decrease significantly with $y$. This decrease above $y/\delta_2 = 4$ corresponds to the increase in $\overline{u'^2} + \overline{w'^2}$ shown in Figure 14. The significantly lower values for $R_{u\theta}$ show that turbulent heat transport is suppressed in the disk boundary layer as hypothesized at the outset.

Figure 15(*b*) shows that the values for $R_{v\theta}$ are small close to the disk but monotonically rise to a constant value between 0.4 and 0.45 in agreement with the 2DTBL value. Again, the small values below $y/\delta_2 = 4$ are surprising because of the strength of the vertical fluctuations indicated in figure 14 and the large temperature fluctuations evident in figure 11. This is another testament to the fact that although there is significant turbulence in the boundary layer, the structures do not seem to be effectively transporting heat. In comparing $R_{v\theta}$ and similar parameters,

$$A_\theta = \frac{\overline{v'\theta'}}{\theta'\left(k^2\right)^{1/2}} \quad \text{and} \quad A_{1\theta} = \frac{\overline{v'\theta'}}{\theta'\left(\overline{u'v'}^2 + \overline{v'w'}^2\right)^{1/4}},$$

to 2DTBL values, it was found that normalizing the vertical heat flux by $v'$ or the wall-parallel shear stress worked well in generalizing parameters, but using $k^2$ or other quantities containing $u'$ and $w'$ did not work.

The turbulent Prandtl number is defined as the ratio of the eddy diffusivity for momentum to the eddy diffusivity for heat, or

$$Pr_t = \frac{\varepsilon_M}{\varepsilon_H} = \frac{-\overline{u'v'}/(\partial\overline{U}/\partial y)}{\overline{v'\theta'}/(\partial\overline{T}/\partial y)}$$

This is not a rigorous definition for $Pr_t$ in a 3DBL, where strictly speaking $Pr_t$ should be a second-order tensor. However, we are primarily interested in turbulent transport in the vertical direction. The definition above deals solely with the vertical direction, and, hence, is simpler and useful for our discussion. The turbulent Prandtl number is typically assumed to be 1 in accordance with the Reynolds analogy. Many 2DTBL

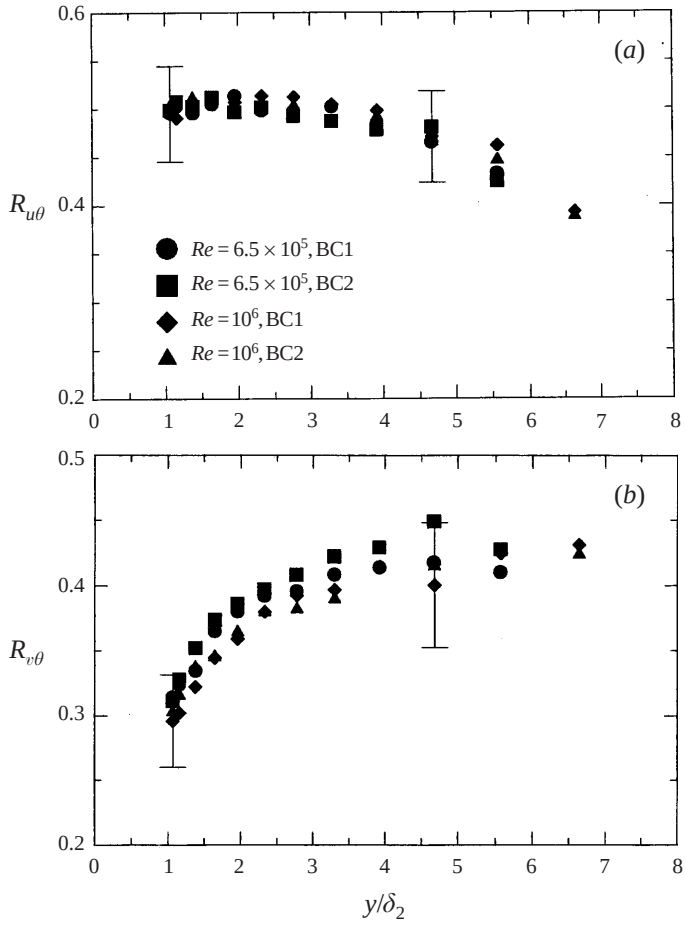


FIGURE 15. The correlation coefficients (*a*) $R_{u\theta}$ and (*b*) $R_{v\theta}$ for all cases. Error bars from table 1.

studies have observed $Pr_t$ to start slightly above 1 around $y/\delta_2 = 1$ and either stay constant or slowly decrease to 0.8 at the edge of the boundary layer. The results of three of these studies taken from Wroblewski & Eibeck (1990) are shown in figure 16. The values for $Pr_t$ in other flows such as the disk flow are not well known, but are important for modellers who calculate $\varepsilon_H$ from $Pr_t$ and $\varepsilon_M$. For instance, Ong & Owen (1991) assumed $Pr_t = 0.9$ in their calculation of the turbulent disk flow. The measurements presented in figure 16 show that $Pr_t$ decreases monotonically in the disk boundary layer reaching levels around 0.5 in the outer layer. The assumption of $Pr_t \approx 0.9$ is consistent with the data below $y/\delta_2 = 4$, but this level is too high over most of the outer layer.

An objective of this experiment was to evaluate the effects that the three-dimensionality has on the turbulent heat flux and the wall-parallel shear stress. Since $Pr_t$ in the disk flow is slightly lower than the measurements of Wroblewski and even smaller than the other measurements made in 2DBLs, the results indicate that the diffusivity for momentum is reduced more than the diffusivity for heat. However, considering the large uncertainty associated with both the present and previous turbulent Prandtl

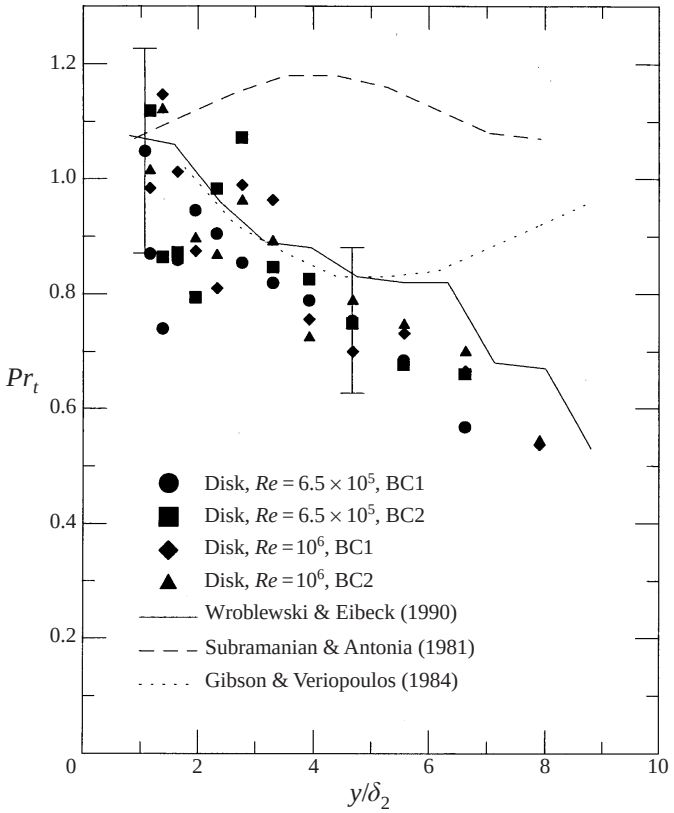


FIGURE 16. The turbulent Prandtl number ($Pr_t$) for all cases compared to results from several 2DBL studies. Error bars indicate uncertainty from table 1.

number measurements, this conclusion must be considered tentative. The conclusion is supported by structural information discussed in the following section.

## 4. Quadrant analysis

Quadrant analysis similar to that of Lu & Willmarth (1973) was used to help illuminate the differences between the turbulent heat flux and the turbulent shear stress made evident in the results for $Pr_t$. In the discussion that follows, $u'$, $v'$, and $\theta'$ denote instantaneous fluctuations measured with the heat flux probe aligned with the mean streamwise direction. The measurements for the shear stress, $\overline{u'v'}$, represent the vector magnitude of the shear stress in the mean streamwise direction. The data presented in this section are from the $Re = 6.5 \times 10^5$ case with BC1, but they are representative of both boundary conditions and Reynolds numbers studied. The results from two positions for the probe are discussed: $y/\delta_2 = 1.11$ ($y^+ = 123$) which is denoted by $I$ and $y/\delta_2 = 5.83$ ($y^+ = 645$) which is denoted by $II$. The time records, which were originally sampled at 20 kHz, were downsampled to produce a total of 10 300 samples for each case.

Figure 17 shows the $(u', v')$-plane with a hole region as defined by Lu & Willmarth. The hole region is the area where $u'v'$ or $v'\theta'$ satisfies the condition $|u'v'| \leqslant H(\overline{u'^2})^{1/2}(\overline{v'^2})^{1/2}$, or $|v'\theta'| \leqslant H(\overline{v'^2})^{1/2}(\overline{\theta'^2})^{1/2}$, respectively, where $H$ is a scalar representing the strength of a stress or heat flux producing event. The negative sign for the

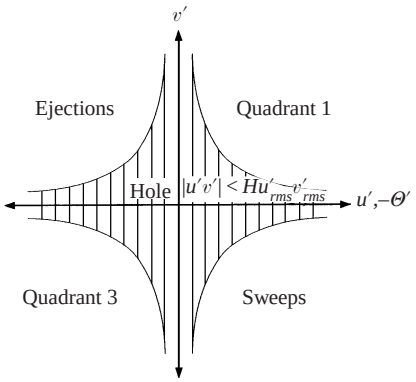


FIGURE 17. Definition of the five regions in the $(u', v')$-plane used in the quadrant analysis of Lu & Willmarth (1973). The fifth region, or hole, is the striped area.

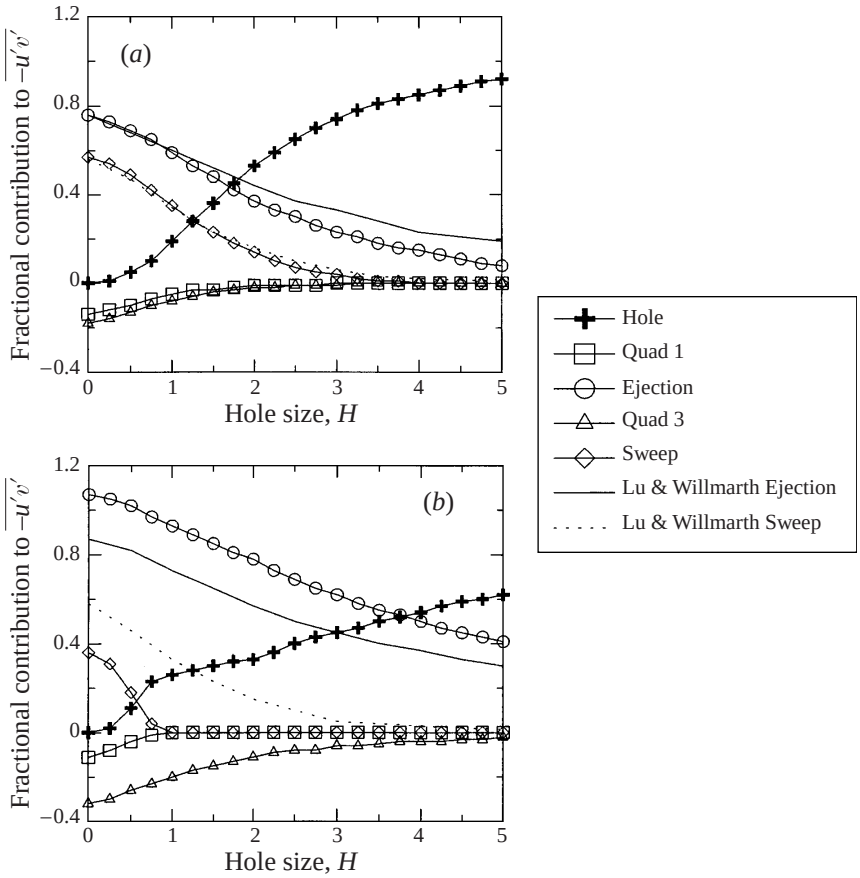


FIGURE 18. The fractional contributions to $-\overline{u'v'}$ from the four quadrants and the hole for varying hole sizes at (*a*) $y/\delta_2 = 1.1$ and (*b*) $y/\delta_2 = 5.8$ for $Re = 6.5 \times 10^5$. Lu & Willmarth data taken at (*a*) $y/\delta = 0.052$ and (*b*) $y/\delta = 0.823$ for a 2DTBL at $Re_\theta = 4230$.

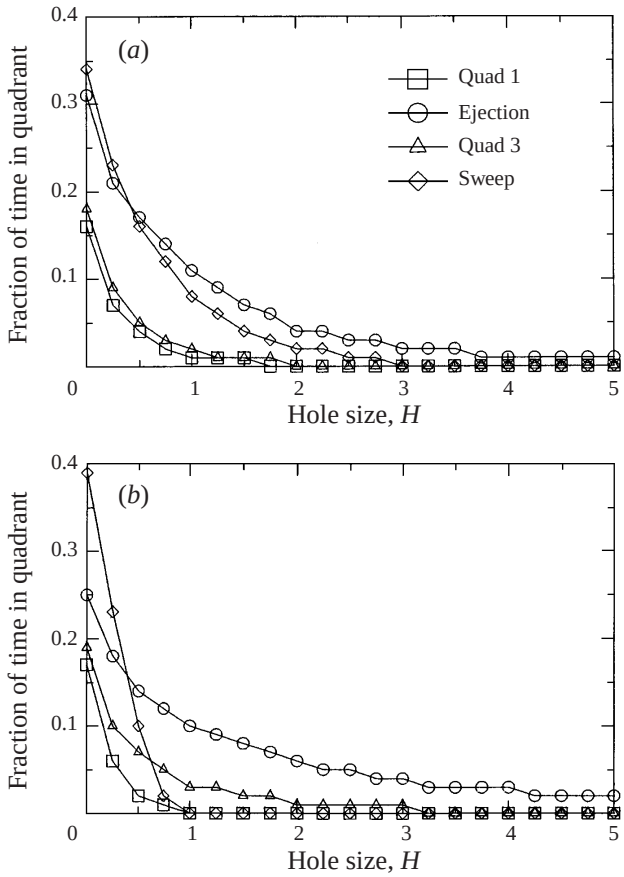


FIGURE 19. The fraction of time the $u'v'$ signal is in each of the four quadrants for varying hole sizes at (*a*) $y/\delta_2 = 1.1$ and (*b*) $y/\delta_2 = 5.8$ for $Re = 6.5 \times 10^5$.

temperature fluctuation is employed such that the ejection and sweep events for the heat flux are associated with quadrants 2 and 4, respectively, just as these events are for the shear stress.

Figure 18(*a*) shows the fractional contribution made to $-\overline{u'v'}$ in each of the five regions for varying hole size at the probe position *I*. The results for the ejection and sweep quadrants closely resemble the data of Lu & Willmarth also shown in figure 18(*a*). Lu & Willmarth's data are from $y/\delta = 0.052$ for a 2DTBL at $Re_\theta = 4230$. This height corresponds to a position inside one momentum thickness. In the disk flow, it is significant that for values of $H > 3$, only ejection events outside the hole region are contributing to the shear stress. Another interesting fact can be seen in a plot of the fraction of time the shear stress is in a particular quadrant. Figure 19(*a*) shows that slightly more sweep events occur than ejection events, but because the sweep events are weaker, the ejections contribute more to the average shear stress.

Figure 18(*b*) shows the fractional contributions at position *II*, which is the outermost point measured with the heat flux probe. The plot looks substantially different than the position closer to the wall and also much different than Lu & Willmarth's 2DBL data from $y/\delta = 0.823$. A large percentage of the contributions come from the ejection quadrant while the sweep quadrant contributes only 35%. This small

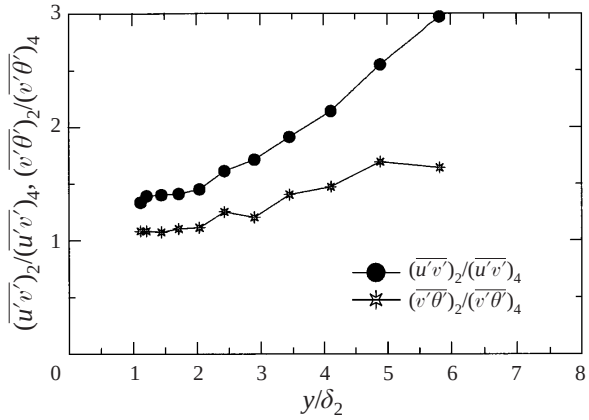


FIGURE 20. The ratios of the shear stress and heat flux contributions from quadrant 2 (ejection quadrant) to the contributions of quadrant 4 (sweep quadrant) across the boundary layer for $Re = 6.5 \times 10^5$.

contribution is not due to the infrequency of sweep events. Rather, it is due to their reduced strength. Above $H = 1$, there are no sweep events, but even for $H = 5$, ejection events occur over 1% of the time. Another interesting result is that quadrant 3 makes a larger negative fractional contribution than it did close to the disk. Figure 19($b$) shows the fraction of time the signal spends in each quadrant for position $II$. It shows the remarkable result that sweeps occur nearly 40% of the time compared to only 25% for ejections, yet the ejections contribute nearly three times as much to the average shear stress.

Another interesting result is obtained by calculating the ratio of the contributions from the ejection and sweep events for hole size $H = 0$. Lu & Willmarth found this ratio to be nearly constant and equal to 1.35 across the boundary layer. Figure 20 shows that in the disk boundary layer, this ratio starts around 1.3 but quickly increases with distance from the wall. The same ratio for vertical heat flux, however, stays relatively constant between 1.1 and 1.6 indicating that the changes affecting the shear stress are having only small effects on the heat flux.

Figure 21($a$) shows the fractional contribution from the quadrants to $\overline{v'\theta'}$ at position $I$. Note that ejections and sweeps contribute nearly equally at this level in the boundary layer as do quadrants 1 and 3. Also noteworthy is the fact that both sweep and ejection events share responsibility for $\overline{v'\theta'}$ even at large values of $H$, and, as figure 22($a$) shows, both types of events occur with nearly equal frequency.

Figure 21($b$) shows the fractional contributions for position $II$. Just as we saw in the $u'v'$ case, the sweep contribution is reduced, but, as is evident in Figure 22($b$), more sweeps occur than ejections. Sweeps do, however, remain important for $H < 2.5$. It is also interesting that the contribution from quadrant 3 remains small. The differences between the results for the shear stress and heat flux events at this height correlate well with the reduced values for $Pr_t$ in the outer portion of the flow. At this height, the turbulent structures are changed such that the ability to mix low- and high-speed parcels of fluid is reduced while the effect on the transport of high- and low-temperature fluid is less significant.

Quadrant analysis similar to that of Perry & Hoffmann (1976) was performed to investigate the relationship between shear stress and heat flux events. Using their definitions, $\{U_i\}$ represents an event in the $i$th quadrant of the $(u', v')$-plane and $\{\Theta_j\}$

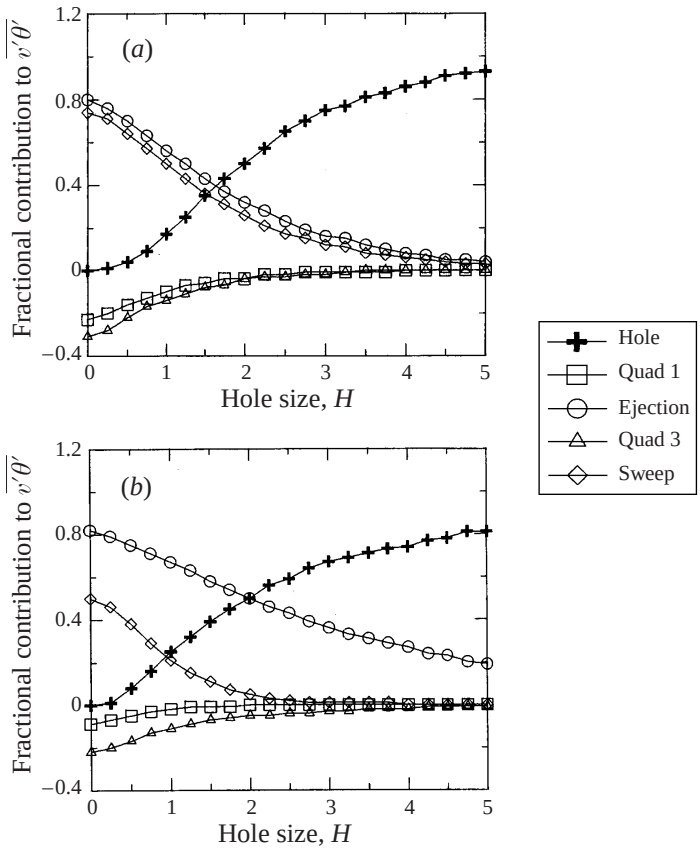


FIGURE 21. The fractional contributions to $\overline{v'\theta'}$ from the four quadrants and the hole for varying hole sizes at (*a*) $y/\delta_2 = 1.1$ and (*b*) $y/\delta_2 = 5.8$ for $Re = 6.5 \times 10^5$.

represents an event in the $j$th quadrant of the $(v', \theta')$-plane. The superscripts $I$ and $II$ correspond to the two probe positions discussed above. The fractions of the total time, or probability, for events in each quadrant were

$$P^I[U_i] = \begin{bmatrix} 0.17 \\ 0.31 \\ 0.18 \\ 0.34 \end{bmatrix}, \quad P^{II}[U_i] = \begin{bmatrix} 0.17 \\ 0.25 \\ 0.19 \\ 0.39 \end{bmatrix}, \tag{4.1}$$

$$P^I[\Theta_j] = \begin{bmatrix} 0.17 \\ 0.30 \\ 0.22 \\ 0.31 \end{bmatrix}, \quad P^{II}[\Theta_j] = \begin{bmatrix} 0.15 \\ 0.28 \\ 0.19 \\ 0.38 \end{bmatrix}. \tag{4.2}$$

These results are similar for the $u'v'$ and $v'\theta'$ data at both probe positions and are similar to the values observed by Perry & Hoffmann in the 2DBL.

Perry & Hoffmann also calculated the simultaneity of $\{U_i\}$ and $\{\Theta_j\}$ events. They defined simultaneity as

$$Q_{ij} = P[U_i \cap \Theta_j].$$

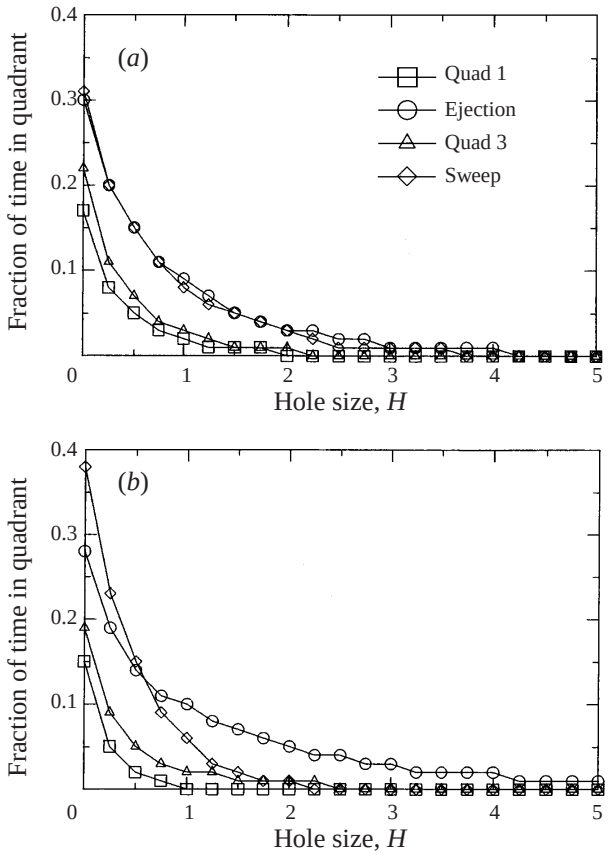


FIGURE 22. The fraction of time the $v'\theta'$ signal is in each of the four quadrants for varying hole sizes at (*a*) $y/\delta_2 = 1.1$ and (*b*) $y/\delta_2 = 5.8$ for $Re = 6.5 \times 10^5$.

The present results for $Q_{ij}$ are

$$Q_{ij}^{I} = \begin{bmatrix} 0.10 & 0.06 & 0 & 0 \\ 0.07 & 0.24 & 0 & 0 \\ 0 & 0 & 0.13 & 0.06 \\ 0 & 0 & 0.09 & 0.25 \end{bmatrix}, \tag{4.3}$$

$$Q_{ij}^{II} = \begin{bmatrix} 0.09 & 0.08 & 0 & 0 \\ 0.06 & 0.19 & 0 & 0 \\ 0 & 0 & 0.10 & 0.08 \\ 0 & 0 & 0.09 & 0.30 \end{bmatrix}, \tag{4.4}$$

which agree well with Perry & Hoffmann who observed simultaneity for sweeps and ejections about 25% of the time ($Q_{22}^{I}$ and $Q_{44}^{I}$). Note there is a slight decrease in $Q_{22}^{II}$ from 0.24 to 0.19 and a slight increase in $Q_{44}^{II}$ from 0.25 to 0.30 indicating that momentum and thermal sweeps occur simultaneously more often than ejections at this higher position.

Using the probability and simultaneity, it is possible to calculate the conditional probability that a $\{U_i\}$ event will occur given that a $\{\Theta_j\}$ event has occurred. Perry

& Hoffmann represented this as $Q'_{ij}$ and defined it as

$$Q'_{ij} = P[U_i|\Theta_j] = P[U_i \cap \Theta_j]/P[\Theta_j].$$

The results for this are

$$Q'^{I}_{ij} = \begin{bmatrix} 0.59 & 0.20 & 0 & 0 \\ 0.41 & 0.80 & 0 & 0 \\ 0 & 0 & 0.59 & 0.19 \\ 0 & 0 & 0.41 & 0.81 \end{bmatrix}, \tag{4.5}$$

$$Q'^{II}_{ij} = \begin{bmatrix} 0.60 & 0.29 & 0 & 0 \\ 0.40 & 0.68 & 0 & 0 \\ 0 & 0 & 0.53 & 0.21 \\ 0 & 0 & 0.47 & 0.79 \end{bmatrix}. \tag{4.6}$$

These also agree with the results from Perry & Hoffmann and indicate a strong likelihood that the structures in the boundary layer responsible for transporting heat are also transporting momentum. The only difference is the value for $Q'^{II}_{22}$ which is reduced from its typical value of 0.8 to 0.68 indicating that the ejection process high in the boundary layer is different from 2DBL ejections.

To investigate the probability of events with different strengths, Perry & Hoffmann used Lu & Willmarth's idea of a hole size to indicate the strength of an event. They used $\{\check{U}_i\}$ to denote an event for which $|u'v'| \leqslant H(\overline{u'^2})^{1/2}(\overline{v'^2})^{1/2}$ and $\{\check{\Theta}_j\}$ to denote an event for which $|v'\theta'| \leqslant H(\overline{v'^2})^{1/2}(\overline{\theta'^2})^{1/2}$. The probability that $\{\check{U}_i\}$ occurs together with $\{\check{\Theta}_j\}$, given that the heat flux event has occurred, can be represented as

$$R_{ij} = P[\check{U}_i|\check{\Theta}_j] = P[\check{U}_i \cap \check{\Theta}_j]/P[\check{\Theta}_j].$$

Using the same values for $H$ that Perry & Hoffmann used, the results for position $I$ are

$$R^I_{ij} = \begin{bmatrix} 0.06^{**} & 0 & 0 & 0 \\ 0.06^{**} & 0.68 & 0 & 0 \\ 0 & 0 & 0.19^{**} & 0 \\ 0 & 0 & 0 & 0.24 \end{bmatrix} \quad \text{for } H = 2.5, \tag{4.7}$$

and

$$R^I_{ij} = \begin{bmatrix} 0 & 0 & 0 & 0 \\ 0 & 0.62^{*} & 0 & 0 \\ 0 & 0 & 0 & 0 \\ 0 & 0 & 0 & 0 \end{bmatrix} \quad \text{for } H = 4.25. \tag{4.8}$$

One problem with conditioning events on $H$ is that the number of strong events is small. For this reason, the probabilities calculated from less than 100 events (1% of the total number of events) are marked with $*$, and the probabilities calculated from less than 20 events are marked with $**$. Since these events are occurring so infrequently, they have little effect on the overall value for the shear stress and heat flux.

The results at position $I$ for $H = 2.5$ are similar to those from Perry & Hoffmann who observed $R_{22} = 0.76$ compared to our 0.68 and $R_{44} = 0.29$ compared to 0.24. The values in the disk flow are only slightly lower. This is true for $H = 4.25$ as well; the disk value for the ejection quadrant is 0.62, reduced from 0.75 observed by Perry

& Hoffmann. The important result in this case is that there is a high probability that when a strong ejection of high-temperature fluid occurs, a strong ejection of momentum occurs as well. The other important result is that only ejection events occur for high values of $H$.

At position $II$, the results for $R_{ij}$ are different from those of Perry & Hoffmann. These results are

$$R_{ij}^{II} = \begin{bmatrix} 0 & 0 & 0 & 0 \\ 0.50^{**} & 0.68 & 0 & 0 \\ 0 & 0 & 0.55^{*} & 0 \\ 0 & 0 & 0 & 0 \end{bmatrix} \quad \text{for } H = 2.5, \tag{4.9}$$

and

$$R_{ij}^{II} = \begin{bmatrix} 0 & 0 & 0 & 0 \\ 0 & 0.68 & 0 & 0 \\ 0 & 0 & 0.64^{**} & 0 \\ 0 & 0 & 0 & 0 \end{bmatrix} \quad \text{for } H = 4.25. \tag{4.10}$$

These results confirm our previous observations that the sweep and ejection mechanisms have changed at this position. When conditioned on the strength of the event, the probability for sweeps is zero since no $u'v'$ sweeps exist above $H = 1$. There is a high probability that a strong ejection event produces ejections for both momentum and heat.

## 5. Discussion

The turbulent heat fluxes and Reynolds stresses were measured from $y/\delta_2 \approx 1$ to 6 corresponding to $y/\delta_{99} \approx 0.1$ to 0.5. The results show that this part of the boundary layer can be split into an inner region below the approximate height of $y/\delta_2 = 3$ and an outer region above it. In the inner region, the quadrant analysis shows that the fractional contributions from sweeps and ejections to $\overline{u'v'}$ are similar to results in 2DBLs. The probability for a simultaneous ejection or sweep event in the $(u', v')$-plane given that an ejection or sweep has occurred in the $(v', \theta')$-plane was calculated to be 80%. This value is a strong indicator that the same structures are transporting momentum and heat. This is also indicated by $Pr_t$ which is close to a value of 1 inside $y/\delta_2 = 3$.

However, there are differences with 2DBLs in this inner region. Littell & Eaton showed that the $a_1$ parameter has a value of $\approx 0.13$ below $y/\delta_2 = 3$ which is below the typical 2DTBL value of 0.15. The suppressed value was attributed to the effects of three-dimensionality weakening the near-wall vortex structures. The results for the correlation coefficients $R_{v\theta}$ and $R_{u\theta}$ support their findings. $R_{v\theta}$ is reduced well below its two-dimensional value and is seen to rise monotonically as $y/\delta_2 = 3$ is approached. This parameter is typically constant across the two-dimensional boundary layer. The behaviour of this parameter suggests that close to the wall, the large amount of random motion associated with the turbulence is poorly organized and results in little net vertical heat flux. The correlation coefficient $R_{u\theta}$ is constant in the inner region, but its value is low compared to 2DBLs.

It is believed that the basic mechanisms for eddy formation in the sublayer are the same as in two-dimensional flat-plate boundary layers. This is supported by the fact that streaky structures are observed to form in three-dimensional boundary layers (Fleming & Simpson 1994) and that there is an equal likelihood of eddies with

either sign of vorticity being associated with the vertical motion of fluid (Littell & Eaton). However, these structures are quickly changed by the presence of cross-flow. The effectiveness of these eddies in mixing fluid thereby creating shear stress and turbulent heat flux is reduced.

Above $y/\delta_2 = 3$, the quadrant analysis shows considerable differences for the turbulent structures in the outer region. The fractional contribution of ejections begins to dominate the shear stress and, to a lesser extent, the heat flux. Such dominance by $u'v'$ ejections is not observed in 2DBLs and indicates a fundamental change in the dynamics at this level in the disk boundary layer. With the changes in the ejection and sweep mechanisms, the $u'$ p.d.f. becomes increasingly skewed having a dramatic effect on the structure parameter

$$\frac{\overline{u'^2} + \overline{w'^2}}{\overline{v'^2}}$$

which increases rapidly with $y/\delta_2$. It is interesting that the probability of a stress producing sweep conditioned on the occurrence of a sweep in the $(v', \theta')$-plane maintains its 0.80 value, but the same conditional probability for ejections has decreased to 0.68. This indicates that shear stress and turbulent heat flux events are not as closely associated as they were in the inner region. Evaluating this change using the results for the fractional contributions to $\overline{u'v'}$ and $\overline{v'\theta'}$, it is seen that the transport of momentum has been altered more than the transport of heat flux. Such a conclusion is supported by the behaviour of the turbulent Prandtl number which decreases with $y/\delta_2$ and drops slightly below the 2DTBL values. Moreover, the dominance of the ejection events helps explain the lack of a wake profile in the mean tangential velocity since the outer layer is dominated by slow fluid coming from the wall. Similarly, the importance of both ejection and sweep events for $\overline{v'\theta'}$ helps explain the high values for the temperature fluctuations and the wake profiles in the mean temperature data.

The characteristics of the outer layer in the disk boundary layer are partly due to the three-dimensionality changing the evolution of the eddies in the inner region but are also due to the nature of the disk flow in which velocity grows linearly with radius. As the eddies grow and are convected downstream, they find themselves over a region of higher velocity. This means they are weak compared to younger turbulent eddies originating at this outer radial position. According to the quadrant analysis and values for $R_{v\theta}$, these eddies can transport passive scalars effectively; however, they are less effective at mixing momentum.

## 6. Summary

New data are provided for coupled momentum and thermal transport in a simple 3DTBL, namely, the rotating disk boundary layer. Mean velocity and Reynolds stress measurements agree well with previous isothermal studies showing that temperature may be considered a passive scalar at the low temperature differences of the present experiment. No previous measurements of scalar transport in 3DTBLs existed, but extensive studies of the momentum transport suggested that scalar transport would be reduced relative to 2DTBL levels.

The disk thermal boundary layer exhibits some unique characteristics. The wake region often observed in semi-log plots of mean velocity was absent in the disk data, but there was a significant wake region in the mean temperature data. The turbulent temperature fluctuations have an expected peak near the wall, and, surprisingly, a second peak in the outer regions of the flow. There is a radial turbulent heat flux not

found in 2DTBLs, and $\overline{w'\theta'}$ also peaks in the outer region. In fact, the magnitude of this heat flux is greater than or equal to the vertical heat flux above $y/\delta_2 \approx 3$.

It appears that the disk boundary layer can be separated into two regions at a height of $y/\delta_2 \approx 3$. Below this height, three-dimensionality affects the turbulence by weakening the quasi-streamwise structures responsible for turbulent shear stress and heat flux. This is evident in the values for the $a_1$ parameter and the correlation coefficients $R_{u\theta}$ and $R_{v\theta}$ which have low values compared to 2DTBL results. Moreover, the three-dimensionality seems to affect transport of momentum and heat similarly. This is confirmed by the results for the turbulent Prandtl number, which is near unity low in the boundary layer.

Above $y/\delta_2 \approx 3$, the outer layer exhibits very different behaviour from what is observed in flat-plate 2DTBLs. Quadrant analysis suggests that the root of the differences is in the balance between ejecting and sweeping motions at this height. Ejections of momentum dominate the shear stress with sweeps contributing virtually nothing to the momentum transport. However, both sweeps and ejections contribute to the vertical heat flux. This fundamental change in transport mechanisms manifests itself in many of the unique characteristics of the disk outer layer. Most important are the low values for the turbulent Prandtl number indicating that the transport of momentum is weakened more than the transport of heat.

This work was supported by the Department of Energy Office of Basic Energy Sciences through Grant DE-FG-93ER14317.

## REFERENCES

Abrahamson, S. & Eaton, J. K. 1991 Heat transfer through a pressure-driven three-dimensional boundary layer. *J. Heat Transfer* **113**, 355–362.

Anderson, S. D. & Eaton, J. K. 1989 An experimental investigation of pressure driven three-dimensional boundary layers. *J. Fluid Mech.* **202**, 263–294.

Antonia, R. A., Danh, H. Q. & Prabhu, A. 1977 Response of a turbulent boundary layer to a step change in surface heat flux. *J. Fluid Mech.* **80**, 153–177.

Blair, M. F. 1981 Velocity and temperature profile data for accelerating, transitional boundary layers. Final Data Report-Vol. II. *United Technologies Research Center Rep.* R81-914388-16.

Blair, M. F. & Bennett, J. C. 1987 Hot-wire measurements of velocity and temperature fluctuations in a heated turbulent boundary layer. *J. Phys.* E: *Sci. Instrum.* **20**, 209–216.

Bradshaw, P. & Pontikos, N. S. 1985 Measurements in the turbulent boundary layer on an 'infinite' swept wing. *J. Fluid Mech.* **159**, 105–130.

Chiang, C. & Eaton, J. K. 1993 An experimental investigation of corotating disks and single disk flow structures. *Stanford Univ. Dept. of Mechanical Engineering, Thermosciences Div. Rep.* MD-62.

Cobb, E. C. & Saunders, O. A. 1956 Heat transfer from a rotating disk. *Proc. R. Soc. Lond.* A **236**, 343–351.

Elkins, C. J. & Eaton, J. K. 1994 Heat transfer measurements in the boundary layer on a rotating disk. In *General Papers in Heat and Mass Transfer, Insulation, and Turbo machinery* (ed. S. H. Chan *et al.*). ASME HTD – Vol. 271, pp. 193–200.

Elkins, C. J. & Eaton, J. K. 1997 Heat transfer in the rotating disk boundary layer. *Stanford Univ. Dept. of Mechanical Engineering, Thermosciences Div. Rep.* TSD-103.

Fleming, J. & Simpson, R. 1994 Experimental investigation of the near wall flow structure of a low Reynolds number 3-D turbulent boundary layer. *AIAA Paper* 94-0649.

Gessner, F. B. & Moller, G. L. 1971 Response behaviour of hot wires in shear flow. *J. Fluid Mech.* **40**, 449–468.

Gibson, M. M. & Verriopoulos, C. A. 1984 Turbulent boundary layer on a mildly curved surface: Part 2: temperature field measurements. *Exps. Fluids* **2**, 73–80.

Guitton, D. E. & Patel, R. P. 1969 An experimental study of the thermal wake interference

between closely spaced wires of a X-type hot-wire probe. *McGill Univ. Mechanical Engineering Research Lab. Rep.* 69-7.

Johnston, J. P. & Flack, K. A. 1996 Advances in three-dimensional turbulent boundary layers with emphasis on the wall-layer regions. *Trans. ASME*: *J. Fluids Engng* **118**, 219.

Kays, W. M. & Crawford, M. E. 1980 *Convective Heat and Mass Transfer*. McGraw-Hill.

Klebanoff, P. S. 1954 Characteristics of turbulence in a boundary layer with zero pressure gradient. *NACA TN* 3178 (superseded by *NACA Rep.* 1247).

Ligrani, P. M. & Bradshaw, P. 1987*a* Spatial resolution and measurements of turbulence in the viscous sublayer using subminiature hot-wire probes. *Exps. Fluids* **5**, 407–417.

Ligrani, P. M. & Bradshaw, P. 1987*b* Subminiature hot-wire sensors: development and use. *J. Phys.* E **20**, 323–332.

Littell, H. S. & Eaton, J. K. 1991 An experimental investigation of the three-dimensional boundary layer on a rotating disk. *Stanford Univ. Dept. of Mechanical Engineering, Thermosciences Div. Rep.* MD-60.

Littell, H. S. & Eaton, J. K. 1994 Turbulence characteristics of the boundary layer on a rotating disk. *J. Fluid Mech.* **266**, 175–207.

Lu, S. S. & Willmarth, W. W. 1973 Measurements of the structure of the Reynolds stress in a turbulent boundary layer. *J. Fluid Mech.* **60**, 481–511.

McComas, S. T. & Hartnett, J. P. 1970 Temperature profiles and heat transfer associated with a single disk rotating in still air. *Proc. Fourth Intl Heat Transfer Conf., Versailles,* vol. 3, p. FC7.7.

Nakayama, A. & Westphal, R. V. 1986 The effects of sensor length and spacing on X-wire measurements in a boundary layer. *NASA TM* 88352.

Ong, C. L. & Owen, J. M. 1991 Computation of the flow and heat transfer due to a rotating disc. *Intl J. Heat Fluid Flow* **12**, 106–115.

Perry, A. E. & Hoffmann, P. H. 1976 An experimental study of turbulent convective heat transfer from a flat plate. *J. Fluid Mech.* **77**, 355–368.

Popiel, C. O. & Boguslawski, L. 1975 Local heat-transfer coefficients on the rotating disk in still air. *Intl J. Heat Mass Transfer* **18**, 167–170.

Strohl, A. & Comte-Bellot, G. 1973 Aerodynamic effects due to configuration of X-wire anemometers. *Trans. ASME*: *J. Appl. Mech.* **40**, 271–277.

Subramanian, C. S. & Antonia, R. A. 1981 Effect of Reynolds number on a slightly heated turbulent boundary layer. *Intl J. Heat Mass Transfer* **24**, 1833–1846.

Tadros, S. E. & Erian, F. F. 1983 Heat and momentum transfer in the turbulent boundary layer near a rotating disk. *ASME Paper* 83-WA/HT-6.

Volino, R. J. & Simon, T. W. 1994 Velocity and temperature profiles in turbulent boundary layer flows experiencing streamwise pressure gradients. In *Fundamentals of Heat Transfer in Forced Convection 1994.* ASME HDT – Vol. 285, pp. 17–24.

Wroblewski, D. E. & Eibeck, P. A. 1990 An experimental investigation of turbulent heat transport in a boundary layer with an embedded streamwise vortex. PhD Thesis, University of California at Berkeley, Mechanical Engineering Department.

Wyngaard, J. C. 1968 Measurements of small-scale turbulence structure with hot wires. *J. Phys.* E **1**, 1105–1108.